Structure and Importance of the Dimerization Domain in Elongation Factor Ts from *Thermus thermophilus*[†,‡]

Youxing Jiang,[§] Steffen Nock,[∥] Martina Nesper,[∥] Mathias Sprinzl,[∥] and Paul B. Sigler*[,⊥]

Department of Chemistry and Department of Molecular Biophysics and Biochemistry and the Howard Hughes Medical Institute, Yale University, New Haven, Connecticut 06520, and Laboratorium für Biochemie, Universitat Bayreuth, Bayreuth, Germany

Received April 16, 1996; Revised Manuscript Received May 30, 1996[⊗]

ABSTRACT: Elongation factor Ts (EF-Ts) functions as a nucleotide-exchange factor by binding elongation factor Tu (EF-Tu) and accelerating the GDP dissociation from EF-Tu; thus EF-Ts promotes the transition of EF-Tu from the inactive GDP form to the active GTP form. *Thermus thermophilus* EF-Ts exists as a stable dimer in solution which binds two molecules of EF-Tu to form a (EF-Tu·EF-Ts)$_2$ heterotetramer. Here we report the crystal structure of the dimerization domain of EF-Ts from *T. thermophilus* refined to 1.7 Å resolution. A three-stranded antiparallel β-sheet from each subunit interacts to form a β-sandwich that serves as an extensive dimer interface tethered by a disulfide bond. This interface is distinctly different from the predominantly α-helical one that stabilizes the EF-Ts dimer from *Escherichia coli* [Kawashima, T., et al. (1996) *Nature 379*, 511−518]. To test whether the homodimeric form of *T. thermophilus* EF-Ts is necessary for catalyzing nucleotide exchange, the present structure was used to design mutational changes within the dimer interface that disrupt the *T. thermophilus* EF-Ts dimer but not the tertiary structure of the subunits. Surprisingly, EF-Ts monomers created in this manner failed to catalyze nucleotide exchange in EF-Tu, indicating that, *in vitro*, *T. thermophilus* EF-Ts functions *only* as a homodimer.

Elongation factor Tu (EF-Tu) and elongation factor Ts (EF-Ts) are proteins which participate in bacterial protein synthesis (Miller & Weissbach, 1977). EF-Tu is a representative member of the GTPase superfamily whose activity is controlled by the state of a bound guanine nucleotide (Bourne et al., 1990, 1991). EF-Tu is inactive in the GDP-bound state. Binding of EF-Ts to EF-Tu·GDP accelerates the release of GDP and the conversion of the EF-Tu from the inactive GDP-bound state to the active GTP-bound state (Arai et al., 1972, 1974a,b, 1978; Ruusala et al., 1982; Romero et al., 1985; Eccleston et al., 1988). In the active GTP-bound state, the binary complex (EF-Tu·GTP) binds aminoacyl-tRNA (aa-tRNA) and brings the aa-tRNA to the A site of the ribosome for entry into the elongation step of protein synthesis. Hydrolysis of the bound GTP releases EF-Tu·GDP from the ribosome, leaving the aminoacyl-tRNA bound to the ribosomal A site.

In contrast to EF-Ts, EF-Tu has been extensively studied, and crystal structures of EF-Tu have been solved in the GDP-bound form (Jurnak, 1985; Kjeldgaard & Nyborg, 1992), the GTP-bound form (Kjeldgaard et al., 1993; Berchtold et al., 1993), and in a ternary complex with aminoacyl-tRNA and a nonhydrolyzable GTP analogue (Nissen et al., 1995). Recently, the structure of EF-Ts from *Escherichia coli* has been solved to 2.5 Å in a complex with EF-Tu (Kawashima et al., 1996). This structure shows the stereochemical details of EF-Ts interactions with EF-Tu and suggests a mechanism for the release of GDP in EF-Tu. Whereas there are similarities in sequence between *E. coli* and *Thermus thermophilus* EF-Ts, there are also substantial differences in the polypeptides' length and sequence that require structural comparison in three dimensions to understand the relationship between these factors in functional and evolutionary terms.

EF-Ts from *T. thermophilus* forms a homodimer in solution (Arai et al., 1978; Blank et al., 1996). Here we present a high-resolution (1.7 Å) crystal structure of homodimeric EF-Ts where residues 1−50 have been removed by an endogenous protease. This amino-terminal segment is involved in the binding of EF-Tu (Blank et al., 1996), a conclusion supported by analogy with the *E. coli* EF-Tu·EF-Ts crystal structure (Kawashima et al., 1996). However, the deletion of these 50 residues does not interfere with dimerization (Blank et al., 1996). The crystal structure of the truncated form of *T. thermophilus* EF-Ts gives us a clear and detailed view of the interactions that stabilize the dimer including a disulfide bond, van der Waals contacts of hydrophobic residues, and hydrogen bonding. The dimer interface visualized in the crystal structure provides a stereochemical framework for the design of mutational changes in EF-Ts subunits which disrupt the dimer but not the tertiary structure of the subunits. These mutational changes were used to probe the importance of EF-Ts dimerization in the EF-Ts-catalyzed GDP/GTP exchange in EF-Tu.

MATERIALS AND METHODS

Crystallization and Data Collection. *T. thermophilus* EF-Ts was expressed in soluble form in *E. coli*, purified to

[†] The work at Yale was supported by NIH Grant GM22324 to P.B.S. and at Bayreuth by DFG Grant Sp 243/8-1 to M.S.

[‡] The atomic coordinates of the structure have been deposited with the Protein Data Bank at Brookhaven National Laboratory. The identification code for the entry is 1TFE.

* To whom correspondence should be addressed at the Department of Molecular Biophysics and Biochemistry, Yale University, 260 Whitney Ave., JWG 421, P.O. Box 208114, New Haven, CT 06520-8114.

[§] Department of Chemistry, Yale University.

[∥] Laboratorium für Biochemie, Universitat Bayreuth.

[⊥] Department of Molecular Biophysics and Biochemistry and the Howard Hughes Medical Institute, Yale University.

[⊗] Abstract published in *Advance ACS Abstracts,* July 15, 1996.

S0006-2960(96)00918-X CCC: $12.00

Table 1: Data Collection Statistics

crystals	source[a]	resolution (Å)	R_{sym}[b] (%)	completeness[c] (%)
parent 1	CHESS A1	2.0	5.9	93.7 (88.6)
parent 2	NSLS X25	1.6	6.8	93.5 (85.9)
Hg derivative	CHESS A1	2.0	5.5	81.5 (69.0)
Os derivative	Raxis II	2.4	7.6	78.5 (69.2)

[a] CHESS A1, Cornell High Energy Synchrotron Source beamline A1, with CCD detector, $\lambda = 0.908$ Å; NSLS X25, National Synchrotron Light Source beamline X25, with Fuji image plates, $\lambda = 0.95$ Å; Raxis II, Rigaku R-AXIS II image plates, with Cu Kα radiation from a Rigaku 2000 generator, $\lambda = 1.54$ Å. [b] $R_{sym} = \sum|I_i - \langle I_i\rangle|/I_i$, where $\langle I_i\rangle$ is the average intensity over symmetry and Friedel equivalents. [c] Numbers in parentheses indicate data completeness in the last resolution shell.

homogeneity as described (Blank et al., 1995), and crystallized by hanging-drop vapor diffusion. Five-microliter drops containing 16 mg/mL protein in 10 mM Tris·HCl, pH 7.5, were mixed with an equal volume of a reservoir solution containing 10% poly(ethylene glycol) 3000 (PEG3000), 40 mM $CaCl_2$, and 100 mM Tris·HCl, pH 8.0, and equilibrated over the reservoir at 18 °C. Hexagonal-shaped crystals appeared after about a week and grew to a size of 0.2 mm × 0.2 mm × 1.0 mm. Analysis of the protein in the crystals by SDS−polyacrylamide gel electrophoresis indicated that EF-Ts had been proteolytically truncated during the equilibration period. The amino acid sequence of the truncated EF-Ts from dissolved crystals showed that the cleavage site is after Lys50 (data not shown). Crystals of the truncated EF-Ts containing residues 51−196 are in the space group $P3_121$, $a = b = 60.1$ Å, $c = 94.3$ Å, and contain one truncated EF-Ts subunit per asymmetric unit. The crystals were transferred to a microdialysis button containing 15% PEG3000, 40 mM $CaCl_2$, and 100 mM Tris·HCl, pH 8.0, and dialyzed against a solution of 20% PEG3000, 40 mM $CaCl_2$, and 100 mM Tris·HCl, pH 8.0, for 12 h, then against a solution of 20% PEG3000, 10% 2-methyl-2,4-pentanediol (MPD), 40 mM $CaCl_2$, 100 mM Tris·HCl, pH 8.0 for 12 h, and finally against a solution of 20% PEG3000, 20% MPD, 40 mM $CaCl_2$, and 100 mM Tris·HCl, pH 8.0. The final solution was used as stabilizer and cryosolvent. The crystals were removed from the stabilizer in nylon loops and frozen in liquid nitrogen-cooled liquid propane. Two parent data sets were collected: one at the National Synchrotron Light Source (NSLS) X25 beamline ($\lambda = 0.95$ Å) at Brookhaven National Laboratory on Fuji image plates and the other one at the Cornell High Energy Synchrotron Source (CHESS) A1 beamline ($\lambda = 0.908$ Å) using a charge-coupled device (CCD) detector. The crystals were kept frozen at −160 °C under a cold nitrogen stream during data collection. The statistics of the data are summarized in Table 1.

Heavy Atom Derivative Search. A Hg^{2+} (mercuric acetate) derivative was obtained by soaking the crystals in stabilizer plus 0.1 mM mercuric acetate for 1 day. The Hg^{2+} derivative data were collected at the CHESS A1 beamline using a CCD detector. An OsO_4^{2-} derivative was obtained by soaking the crystals in stabilizer plus 10 mM K_2OsO_4 for 3 days. The OsO_4^{2-} derivative data were collected on a Rigaku R-AXIS II image plate detector at Yale University with mirror-focused Cu Kα radiation from a Rigaku 2000 generator. Data statistics are shown in Table 1.

Structure Determination and Refinement. All data sets were processed with DENZO (Otwinowski, 1993) and scaled with SCALEPACK (Otwinowski, 1993). A single Hg^{2+} binding site was found by direct methods, applying SHELXS 86 (Sheldrick, 1990) to the isomophous differences. One OsO_4^{2-} site per asymmetric unit was found by a difference Fourier phased with the Hg^{2+} derivative. The heavy atom derivatives were refined and phases calculated using MLPHARE (Otwinowski, 1991). The phasing statistics are summarized in Table 2.

A 2.5 Å multiple isomorphous replacement (MIR) electron-density map was calculated, and the density was improved by solvent flattening and histogram matching using DPHASE (G. Van Duyne, personal communication). The quality of the electron density map was good, and the side chains of most residues were clear. The original model containing residues 55−196 was built with the program O (Jones, 1991).

All refinement was performed using X-PLOR (Brunger, 1992). The current model, containing residues 55−196 and 259 water molecules, has been refined to 1.7 Å resolution using the data collected at the NSLS X25 beamline with a working R value of 20.7% and free R value of 28.5% for data $>2\sigma$. No electron density was seen for residues 51−54, which are the first four amino acids of the truncated EF-Ts. The geometry of the model is excellent. The refinement results are shown in Table 2.

Construction and Overexpression of EF-Ts Variants. Two residues in *T. thermophilus* EF-Ts were targeted for mutagenesis: leucine-73 to aspartic acid (EF-TsL73D) and cysteine-190 to alanine (EF-TsC190A). For the replacement of leucine-73 by aspartic acid, three synthetic oligodeoxyribonucleotides were designed: one corresponds to the N-terminal part of the *tsf* gene (5′-GACATATGAGCCAAATG-GAACTCAT-3′), the second one corresponds to the C-terminal part of the *tsf* gene (5′-AGGGATCCCGGGTCAGGA-ACTCGCCGGA-3′), and the third one bears the mutagenetic site (5′-CAGTTGAGCTCCACATCGACCCCCACCC GC-TGG-3′; the triplet encoding the mutation is underlined). These oligodeoxyribonucleotides were used for PCR according to the method described by Sarkar and Sommer (1990) with 20 ng of linearized pETTs7 (Blank et al., 1995) as the template. The amplified fragment, digested with *Nde*I and *Bam*HI, was ligated with the linearized expression vector pET28c(+) (Novagen, Madison, WI). The resulting plasmid pET28TsL73D was sequenced and used for transformation of *E. coli* BL21(DE3) (Studier et al., 1990). To replace cysteine-190 with alanine, a *Xba*I/*Bam*HI fragment of pETTs7 (Blank et al., 1995) was cloned in pBluescript II KS+ (Stratagene, La Jolla, CA) for preparing single-stranded DNA. Site-directed mutagenesis was performed according to the method developed by Kunkel et al. (1987) using the oligodeoxyribonucleotide (5′-GTGGTCCGACGCTTCGC-CCGCTTTGAGCT GGGG-3′; the triplet encoding the mutation is underlined) which carries the mutagenic site. After mutagenesis and sequencing, the mutagenized *Xba*I/*Bam*HI fragment was cloned back into a pET3c vector. Standard protocols were followed for DNA handling and bacterial transformation (Sambrook et al., 1989).

Purification of EF-Ts and Its Variants. The wild-type EF-Ts and EF-Ts mutants (EF-TsL73D and EF-TsC190A) from *T. thermophilus* were expressed in *E. coli* BL21(DE3). The purification of EF-TsC190A is the same as for the wild-type EF-Ts including heat denaturation of *E. coli* proteins as previously described (Blank et al., 1995). Due to the

Table 2: Phasing Statistics and Refinement Results

phasing statistics									
resolution (Å)	9.23	6.67	5.22	4.29	3.64	3.16	2.79	2.50	all
phasing power[a]									
Hg derivative	3.72	4.33	4.91	3.16	2.55	2.35	2.45	2.52	2.74
Os derivative	1.96	2.82	2.46	1.57	1.26	1.16	1.21	1.17	1.36
mean figure of merit[b]	0.73	0.80	0.80	0.68	0.61	0.60	0.61	0.59	0.62

refinement result[c]	resolution (Å)	reflections	*R*-factor (%)	free *R*-factor (%)
data $>2\sigma$	8−1.7	19706	20.7	28.5
all data	8−1.7	21390	21.7	29.4

rms deviations:[d] bond lengths 0.011 Å; bond angle 1.5°; improper dihedral angles 1.5°

[a] Phasing power $= \sum|F_H|/\sum| |F_{PH}(obs)| - |F_{PH}(calc)| |$. [b] Figure of merit $= \int P(\phi) \exp(i\phi)\, d\phi / \int P(\phi) d\phi$ in which P is the probability distribution of the phase angle ϕ. [c] The data collected at the NSLS X25 beamline (parent 2 in Table 1) were used for refinement. The data in the 1.6−1.7 Å resolution shell are not of sufficient quality to merit inclusion in the refinement, so the structure was refined to 1.7 Å. [d] rms = root mean square.

thermal instability of EF-TsL73D at temperatures above 60 °C, six histidines were added to the N-terminus (His-tag) which allows purification of the recombinant protein by affinity chromatography on Ni^{2+}−nitrilotriacetic acid (Ni−NTA; Qiagen, Düsseldorf, Germany) without the heat denaturation step. To purify the His-tagged EF-TsL73D, the cells were lysed and the cell extract was centrifuged at 30 000*g*. The supernatant was dialyzed against a buffer containing 50 mM Tris·HCl, pH 7.5, 50 mM KCl, and 10 mM $MgCl_2$ and then applied to a Ni−NTA column. Weakly bound proteins were eluted with 10 mM imidazole. The His-tagged EF-TsL73D mutant was eluted with 500 mM imidazole and applied on a Superdex 200 gel filtration column (2.6 × 60 cm, Pharmacia, Uppsala, Sweden) to separate the complex of *T. thermophilus* EF-TsL73D and endogenous *E. coli* EF-Tu (Arai et al., 1978; Wittinghofer et al., 1983) from the free EF-TsL73D. The fractions containing EF-TsL73D were pooled and dialyzed against a buffer containing 50 mM Tris·HCl, pH 7.5, 50 mM KCl, and 50% glycerol and stored at −20 °C. The purity of EF-Ts and its variants was estimated by SDS−polyacrylamide gel electrophoresis to be greater than 95%.

EF-Ts Activity Assay. EF-Ts catalyzes the exchange of EF-Tu-bound GDP with free GDP. A filter-binding assay was used to measure the EF-Ts activity (Arai et al., 1972). EF-Ts was added to a 100 μL solution containing 1 μM EF-Tu·GDP, 50 mM Tris·HCl, pH 7.5, 10 mM $MgCl_2$, 150 mM NH_4Cl, 5 mM 2-mercaptoethanol, 5 μM [^{3}H]GDP (100 mCi/mmol), and 1 mg/mL bovine serum albumin. The mixture was incubated at 0 °C for 1 min. The reaction was stopped by addition of 1 mL of ice-cold buffer containing 10 mM Tris·HCl, pH 7.5, 10 mM $MgCl_2$, and 10 mM NH_4Cl, followed by filtration through nitrocellulose (Satorius, Göttingen, Germany). The filter was further washed with 1 mL of the same buffer, and the radioactivity retained on the filter was counted to determine EF-Ts activity. One unit of EF-Ts catalyzes the exchange of 1 pmol of EF-Tu-bound GDP in 1 min at 0 °C. The activity test was also performed at 25 °C to have comparable conditions to the gel permeation chromatography.

Gel Permeation Chromatography. The extent of dimerization of EF-Ts and its variants was determined by gel filtration with Superdex 200 (1 × 30 cm, Pharmacia, Uppsala, Sweden) at 25 °C. The protein concentration of the loaded sample was 1 mg/mL, and the column was washed with the buffer containing 50 mM Tris·HCl, pH 7.5, and 150 mM KCl at a flow rate of 0.4 mL/min.

Circular Dichroism Measurements and UV-Monitored Denaturation. The circular dichroism of 30 μM protein in 10 mM potassium phosphate, pH 7.5, and 50 mM KCl was measured in 1 mm path-length cuvettes at 20 °C with a Jasco J600 spectropolarimeter. The spectra were measured six times. Ellipticity is reported as mean residue ellipticity and was calibrated with (+)-10-camphorsulfonic acid.

UV melting curves were measured at a concentration of 20 μM protein in 50 mM Hepes−KOH, pH 7.5, 10 mM $MgCl_2$, and 50 mM KCl over a temperature range of 20−90 °C using a diode array spectrophotometer, Model 8452A (Hewlett Packard, Waldbronn, Germany). The thermal dependence of the absorbent difference at 274 and 286 nm was recorded.

RESULTS

General Features of the Structure. Consistent with solution studies, truncated EF-Ts is an obvious dimer in the crystal structure. The crystallographic dyad corresponds to the molecular dyad, making the crystalline EF-Ts dimer exactly symmetrical. The overall secondary structure of a truncated EF-Ts subunit is formed by three β-strands (β1, β2, and β3), a short α-helix (α1), and four long α-helices (α2, α3, α4, and α5) (Figure 2). The three β-stands constitute an antiparallel β-sheet which forms the dimer interface. The four long helices, α2, α3, α4, and α5, form two antiparallel coiled coils with α2 packing against α5 and α3 against α4. The α2/α5 coil rests against the three-stranded antiparallel β-sheet forming a compact core. The α3/α4 coil protrudes outward, making the molecule elongated.

Dimer Interface. The dimer interface is a three-stranded antiparallel β-sandwich, which buries 2156 Å^2 of otherwise solvent-accessible area. The interactions within the dimer interface are composed of an intersubunit disulfide bond, van der Waals contact between nonpolar surfaces, and hydrogen bonds.

A cysteine (Cys190) from one subunit, located in the middle of β3 and at the edge of the interface, forms a disulfide bond with the corresponding cysteine from the other subunit. A sigmaA weighted $2|F_o| - |F_c|$ electron-density map which minimizes model bias (Read, 1986) clearly shows strong electron density for the intersubunit disulfide *bond* (Figure 3). Analysis of EF-Ts in solution also shows that it is Cys190 that forms the disulfide bond (Blank et al., 1996). In fact, among the EF-Ts sequences shown in Figure 1, Cys190 is unique to *T. thermophilus* EF-Ts.

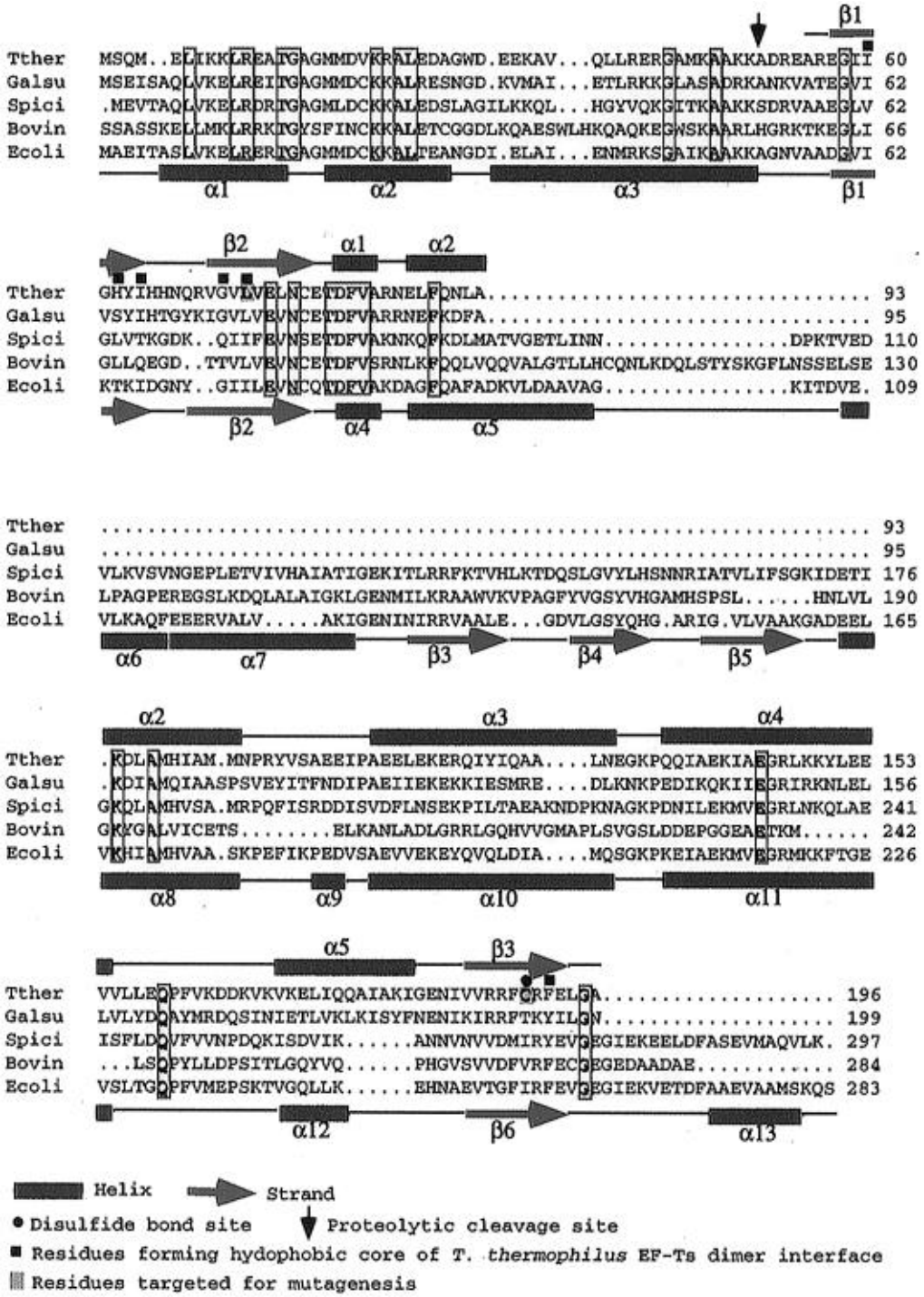

FIGURE 1: Alignment of EF-Ts sequences using GCG Wisconsin Package V8.1 (1995). Symbols (red arrow is a β-strand, green bar is an α-helix) refer to the current structure of the *T. thermophilus* EF-Ts dimerization domain (top) and *E. coli* EF-Ts (bottom). Magenta boxes enclose identical residues. The numbering of *T. thermophilus* EF-Ts was inferred from the gene sequence (Blank et al., 1995). It is possible that in its natural host the terminal formylmethionine is cleaved off in the *T. thermophilus* EF-Ts as is the case for *T. thermophilus* EF-Ts overexpressed in *E. coli* (Blank et al., 1996) which was used in this study. Source of sequence information: *T. thermophilus* (Tther) EF-Ts (Blank et al., 1995), *Galdieria sulphuraria* chloroplast (Galsu) EF-Ts (Kostrzewa & Zetsche, 1993), *Spiroplasma citri* (Spici) EF-Ts (Chevalier et al., 1990), bovine liver mitochondrial (Bovin) EF-Ts (Xin et al., 1995), and *E. coli* (Ecoli) EF-Ts (An et al., 1981).

As the disulfide bond is located at the edge of the dimer interface which is solvent accessible (Figure 4), the modification of the sulfhydryl group with a polar substituent such as a carboxymethyl group can be accommodated by the adduct pointing into the solvent. Indeed the disulfide bond is reactive to both reduction and alkylation under native conditions. Gel permeation chromatography shows that EF-Ts still forms a stable homodimer even after modification of Cys190 (Blank et al., 1996). This suggests that interactions other than the disulfide bond also stabilize the dimer.

The side chains of six residues in the antiparallel β-sheet from one subunit form strong hydrophobic interactions with the corresponding side chains from the opposing subunit. These hydrophobic residues together with the disulfide bond form the core of the dimerization interface around the molecular dyad (Figure 4). Ile60, His62, Ile64, Cys190, and

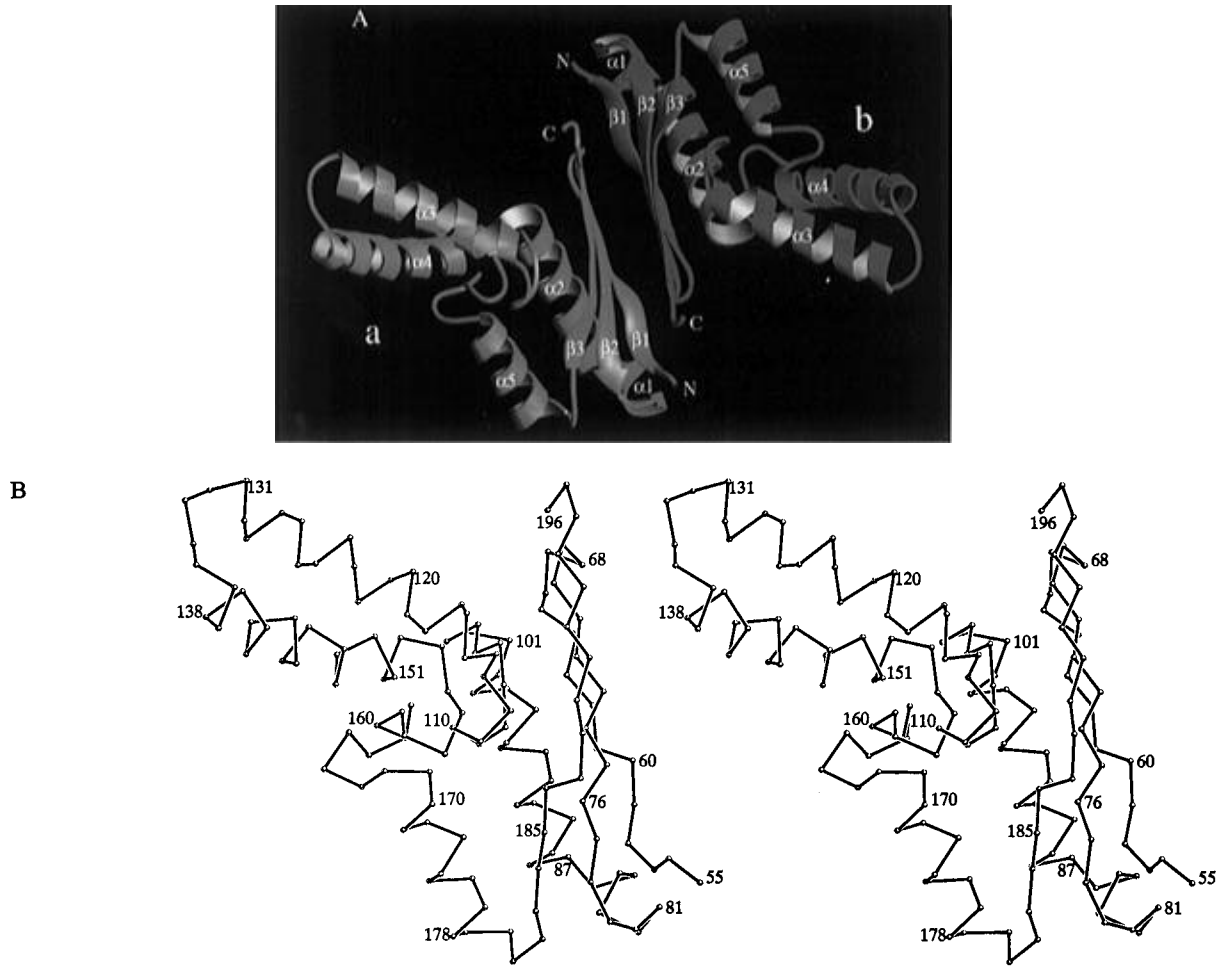

FIGURE 2: Structure of the EF-Ts dimerization domain. (A) Ribbon drawing of the truncated EF-Ts homodimer viewed down the molecular/crystallographic dyad. The N-terminus of the refined crystal structure begins at Ala55. The first four amino acids (residues 51−54) are poorly ordered. (B) Stereoview of the C_α trace of one subunit in the same orientation as subunit a in (A).

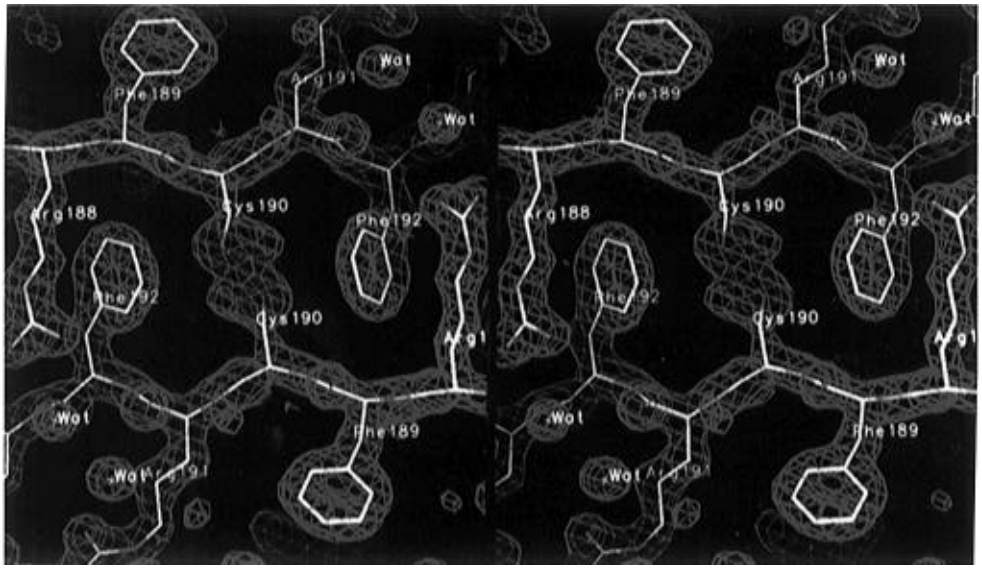

FIGURE 3: SigmaA weighted $2|F_o| - |F_c|$ electron-density map of the region around the disulfide bond (red). The map is contoured at 2.0σ.

Phe192 from each subunit are located at the edge of the hydrophobic core while Gly71 and Leu73 are buried in the middle. Thus, replacement of Leu73 with a charged amino acid might disrupt the hydrophobic core of the interface.

A hydrogen-bonding network, both direct and water mediated, is formed around the hydrophobic core. The hydrogen bonds are clustered in two symmetrically disposed locations on either side of the hydrophobic core. There are two groups of hydrogen bonds within each location as shown in Figure 5.

Mutational Analyses. On the basis of the crystal structure of the EF-Ts dimerization domain, two *T. thermophilus* EF-Ts residues were targeted for change in order to disrupt the dimer interface: cysteine-190 was replaced by alanine (EF-

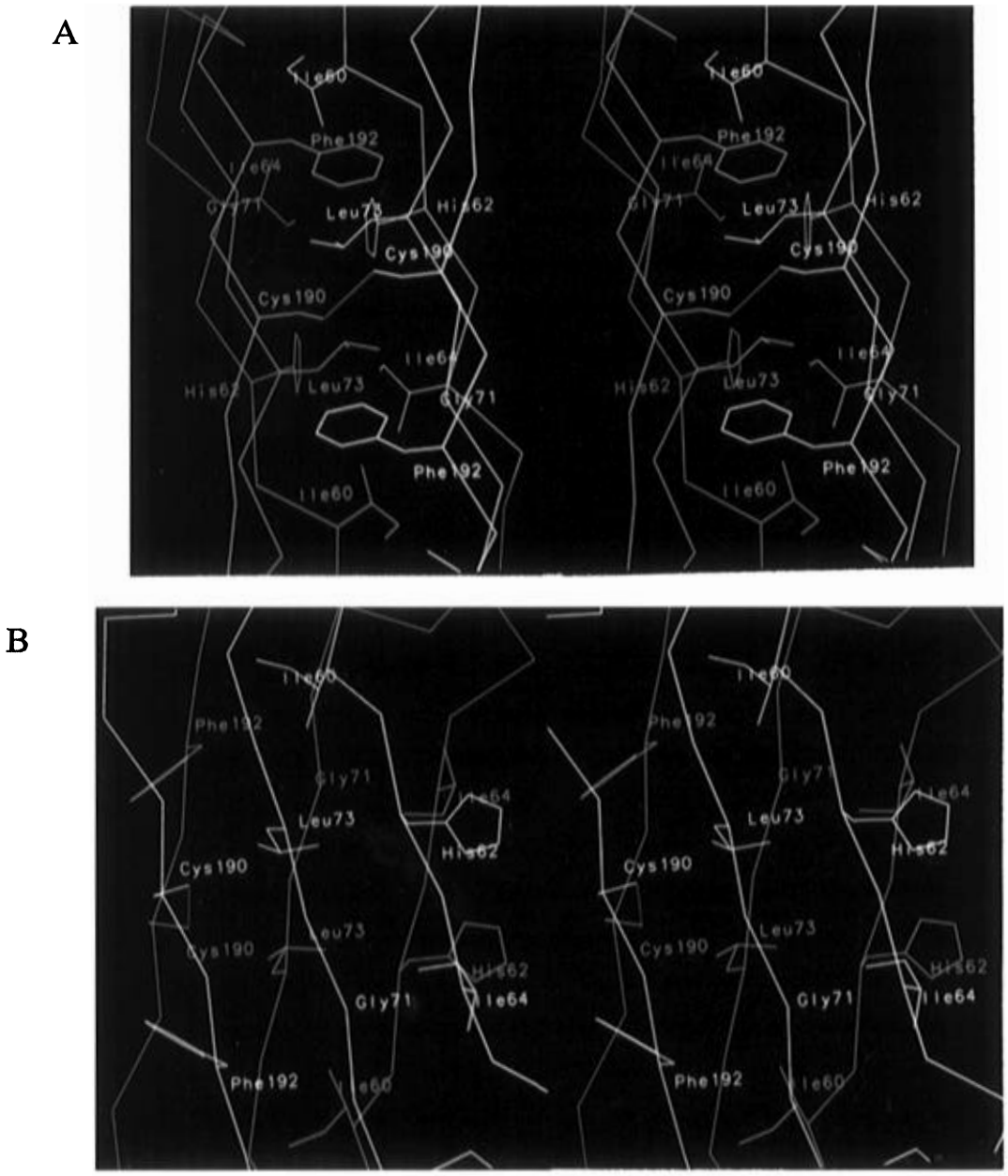

FIGURE 4: Dimer interface. (A) Stereoview of the hydrophobic core along the molecular dyad. (B) Stereoview of the hydrophobic core where the dyad is the horizontal axis in the paper plane. The residues from the two different subunits are in cyan and yellow, respectively, and the disulfide bond is the red line.

TsC190A) to disrupt the disulfide bond and leucine-73 was replaced by aspartic acid (EF-TsL73D) to disrupt the hydrophobic core.

Gel permeation chromatography shows that wild-type *T. thermophilus* EF-Ts forms a dimer and is eluted at an apparent molecular mass of 54 kDa (Figure 6a). EF-TsC190A, in which only the disulfide is disrupted, still forms a dimer (Figure 6b). EF-TsL73D partially disrupts dimer formation in an oxidizing environment (Figure 6c), but no dimer can be detected after treating EF-TsL73D with a reducing agent, 2-mercaptoethanol (Figure 6d), which suggests that a portion of the EF-TsL73D molecules can still form dimers via disulfide bond. These results are consistent with the structure of the EF-Ts dimerization domain which shows that the dimerization interactions involve both noncovalent interactions and a disulfide bond. Disrupting either one alone does not disrupt the dimer completely. The activity of EF-TsL73D was tested with *T. thermophilus* EF-Tu. Under oxidizing conditions, EF-TsL73D possesses about 70% activity as compared to the wild-type protein, but this activity is almost completely lost under reducing conditions and can be regained by reoxidation (Figure 7). These results were obtained at 0 and 25 °C and strongly imply that *T. thermophilus* EF-Ts functions only as a dimer. CD spectroscopy results indicate that the loss of activity of EF-TsL73D under reducing conditions is not due to denaturation of the subunits (data not shown).

Not surprisingly, dimerization enhances the thermal stability of the individual EF-Ts subunit. The wild-type protein does not denature up to 95 °C. Removal of the disulfide bond between the two Cys190 (EF-TsC190A) decreases the melting temperature (T_m) of EF-Ts to 83 °C. EF-TsL73D, in which the hydophobic dimerization interface is disrupted, is less thermostable and can be denatured at a temperature of about 60 °C (Figure 8). The thermal transitions for both mutants are sharp and are at temperatures well above that

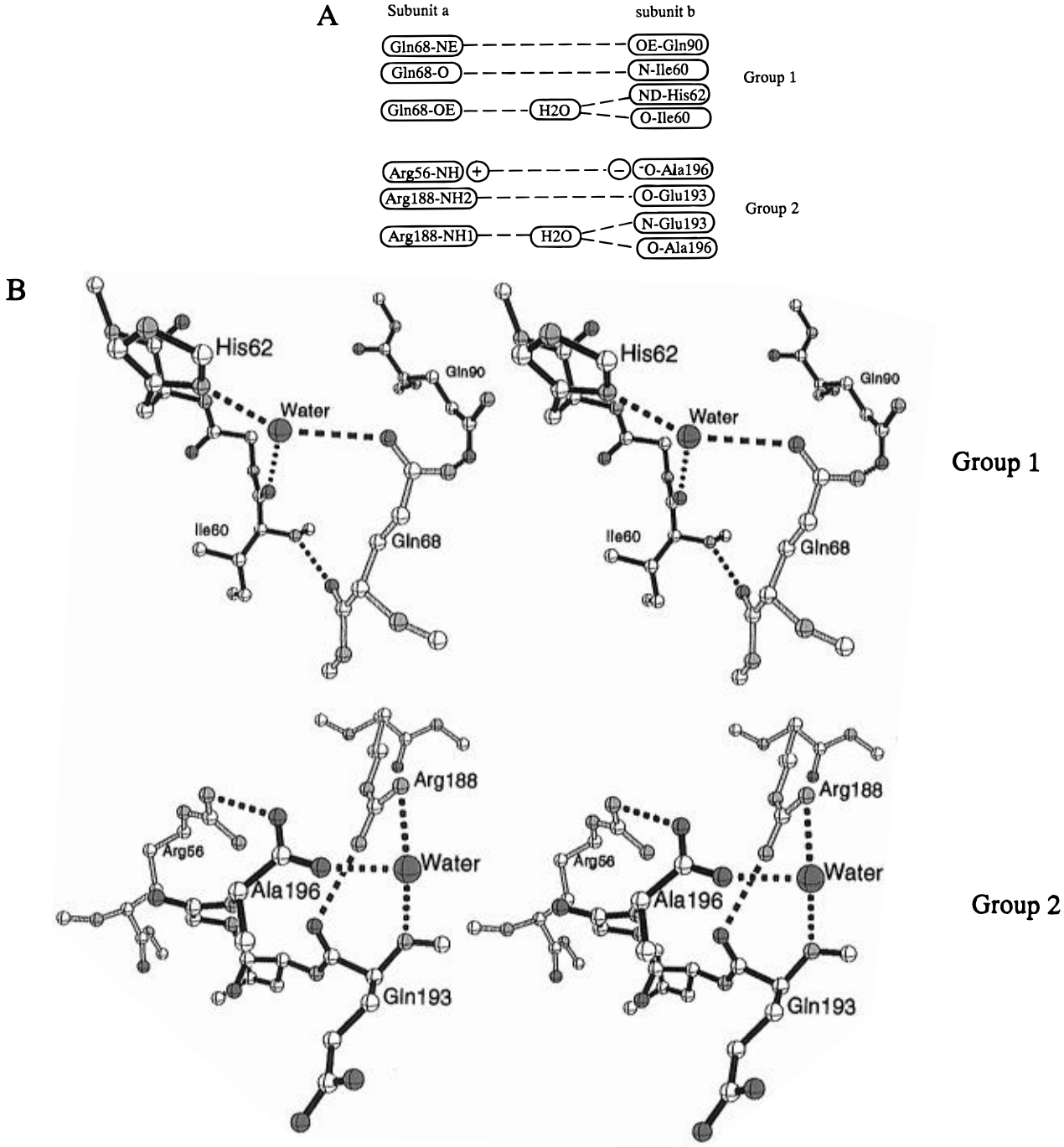

FIGURE 5: Hydrogen-bonding network around the dimerization center. (A) Connectivity scheme of the two groups of hydrogen bonds. (B) Stereoview of the two groups of hydrogen-bonding interactions. The bonds of the two different subunits are colored gray and black. The hydrogen bonds are black dotted lines. Oxygen atoms are in red and nitrogen atoms are in blue.

showing disruption of the dimer and loss of activity of EF-Ts. Taken together with the results of CD spectroscopy, we conclude that it is the disruption of the dimer, not loss of subunit structure, that is responsible for the failure of *T. thermophilus* EF-Ts to catalyze nucleotide exchange. The results of the mutational analyses are summarized in Table 3.

DISCUSSION

We have determined the crystal structure of a truncated form of EF-Ts from *T. thermophilus* in which the N-terminal 50 amino acids were inadvertently removed by endogenous proteolysis during crystallization. The endogenous cleavage site, between Lys50 and Ala51 in a conserved region of sequence 46-KAAKKA-51 (Figure 1), corresponds almost exactly to the trypsin cleavage site observed for EF-Ts from both *T. thermophilus* and *E. coli* (Blank et al., 1996; Bøgestrand et al., 1995), which suggests that in this region the backbone is flexible and at least transiently solvent exposed. The missing N-terminal segment of EF-Ts is required for binding its "substrate", EF-Tu (Blank et al., 1996; Kawashima et al., 1996); hence the truncated crystalline protein cannot catalyze nucleotide exchange. However, loss of the N-terminus has no apparent effect on the stability of the dimer in solution (Blank et al., 1996), and the structure shows the site of N-terminal cleavage to be extended away from the dimer interface. It is therefore unlikely that this deleted region plays a direct role in dimerization.

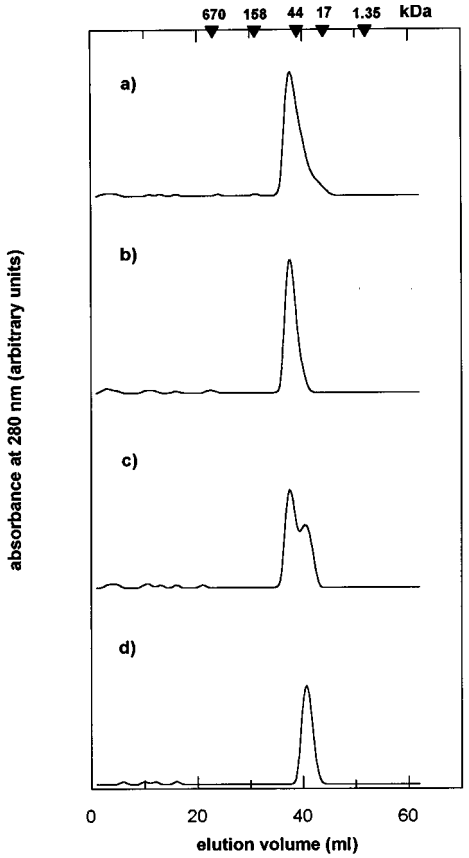

FIGURE 6: Gel permeation chromatography of *T. thermophilus* EF-Ts and its variants. The filled triangles indicate the elution volumes of the standard proteins with corresponding molecular weights. The range of absorbance at 280 nm is between 0 and 0.05. Panels: (a) wild-type EF-Ts; (b) EF-TsC190A; (c) EF-TsL73D; (d) EF-TsL73D in the presence of 50 mM 2-mercaptoethanol.

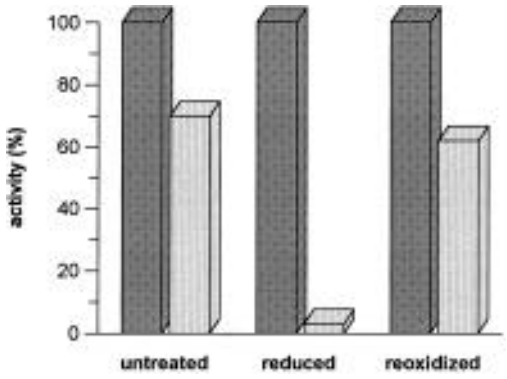

FIGURE 7: Activity of EF-Ts (dark bars) and EF-TsL73D (gray bars) in the absence (presumably oxidizing conditions) and in the presence (reducing conditions) of 50 mM 2-mercaptoethanol. Reduction was achieved by preincubation of the EF-Ts sample with 50 mM 2-mercaptoethanol at 25 °C for 60 min. Reoxidation was achieved by dialyzing the reduced sample against the buffer containing 50 mM Tris·HCl, pH 7.5, and 50 mM KCl.

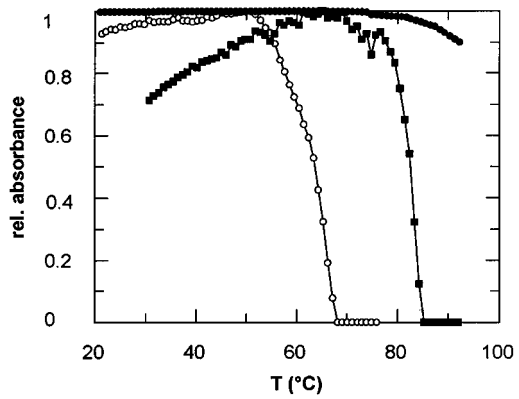

FIGURE 8: Heat denaturation of EF-Ts (●), EF-TsC190A (■), and EF-TsL73D (○) in 50 mM Hepes·KOH, pH 7.5, 10 mM $MgCl_2$, and 50 mM KCl as monitored by the UV absorption difference at 274 and 286 nm.

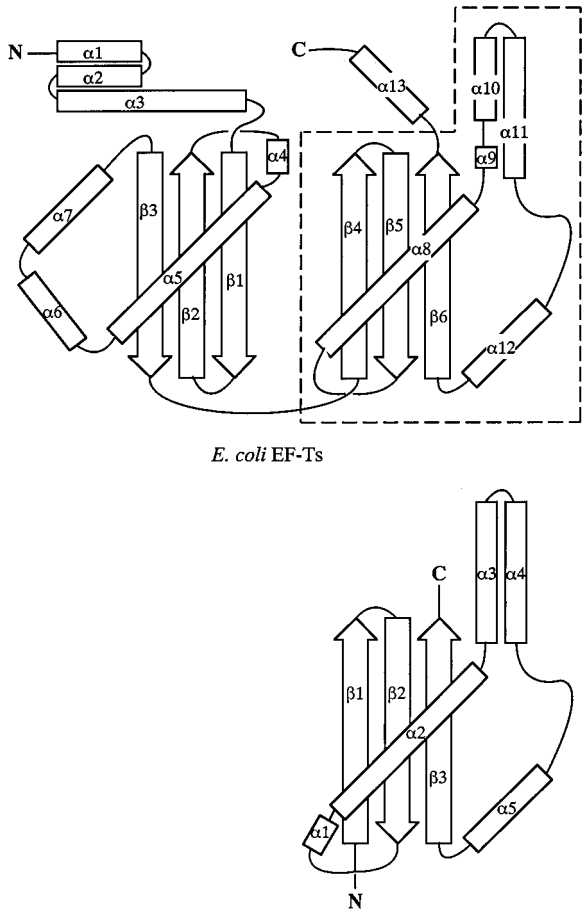

FIGURE 9: Folding pattern of *E. coli* EF-Ts and truncated *T. thermophilus* EF-Ts. The box with dotted lines encloses the C-terminal portion of *E. coli* EF-Ts that has a folding pattern similar to that of the truncated *T. thermophilus* EF-Ts.

It is important to determine the functional significance of the dimerization of EF-Ts from *T. thermophilus.* The high resolution of the truncated EF-Ts structure gives a clear picture of a symmetrical dimer interface which enabled us to design mutants that were likely to disrupt the full-length EF-Ts dimer without interfering with the tertiary structure of the subunits. This task was made easier by the "β-sandwich" nature of the interface; that is, the side chains project outward from the β-sheet to engage the side chains of their dimer-related mate. Two mutations were particularly informative. One mutation (C190A) eliminates the possibility of intersubunit disulfide formation. The other (L73D) inserts a negatively charged side chain into the otherwise hydrophobic core of the dimer interface that provides no access to compensatory positive charge from either a neighboring side chain or ambient counterion. The C190A change supports the biochemical observation that the disulfide bond seen in the crystal structure (under oxidative

Table 3: Summary of Mutational Analyses

sample	EF-Ts	EF-Ts	EF-TsC190A	EF-TsL73D	EF-TsL73D
experimental conditions[a]	unreduced	reduced	unreduced	unreduced	reduced
dimerization interactions[b]	dimer, HP/S−S	dimer, HP	dimer, HP	partially dimer, S−S	monomer
T_m (°C)	95		83	60	
activity	active	active	active	70% active	no activity

[a] Under reduced conditions, 50 mM 2-mercaptoethanol was added to the buffer. [b] HP = hydrophobic interaction; S−S = disulfide bond.

conditions) is not normally required to maintain the dimer in *in vitro* conditions. The L73D change destabilizes the dimer and completely disrupts dimerization if the intersubunit disulfide bond is reduced. Once the dimer is disrupted, EF-Ts loses its capacity to function under conditions where CD spectroscopy shows no evidence of denaturation. Reoxidation of the disulfide bond in EF-TsL73D partially restores its function, to the same extent as it restores dimerization. Since the extensive interactions across the dimer interface are likely to help stabilize the individual subunits, monomeric EF-Ts, as expected, is more easily heat denatured than the dimer (Figure 8). However, the thermal transition of monomeric EF-Ts (EF-TsL73D) occurs at about 60 °C, well above the assay temperature of 0 and 25 °C, and the transition curve is as sharp as that of wild-type EF-Ts (Figure 8). This suggests that monomeric EF-Ts forms a stably folded structure below the transition temperature as confirmed by the CD spectroscopy of these EF-Ts variants.

What special advantage accrues to the EF-Ts-catalyzed nucleotide exchange reaction through the use of a dimeric EF-Ts? It is possible that the (EF-Tu·EF-Ts)$_2$ heterotetramer is formed through dimerization of EF-Ts to increase the stability of the EF-Tu which is unstable in the nucleotide-free state transiently formed during the nucleotide-exchange reaction (Sprinzl & Hilgenfeld, 1993).

Very recently, the crystal structure of the *E. coli* EF-Tu·EF-Ts complex was solved to 2.5 Å (Kawashima et al., 1996). In this structure, *E. coli* EF-Ts also forms a dimer and a heterotetrameric complex with EF-Tu, i.e., (EF-Tu·EF-Ts)$_2$. The dimer interface in *E. coli* EF-Ts is predominantly composed of α-helices instead of β-sheets as is the case for *T. thermophilus* EF-Ts, even though the dimerization domain of *E. coli* EF-Ts is conserved in all EF-Ts sequences (45% identical between *E. coli* and *T. thermophilus* EF-Ts). Of those residues that contribute to intersubunit contacts, all but one are identical or similar to their *T. thermophilus* counterpart. On the other hand, *E. coli* EF-Ts has an internal three-stranded antiparallel β-sandwich which is similar in its conformation to the dimer interface between two *T. thermophilus* EF-Ts subunits. The folding pattern of the *T. thermophilus* EF-Ts subunit in the present crystal structure is remarkably similar to the C-terminal portion of *E. coli* EF-Ts (residues 140−260) as shown in Figure 9. The arrangement of secondary structure elements of the *E. coli* EF-Ts monomer bears a resemblance to the arrangement of secondary structure elements of the *T. thermophilus* EF-Ts dimer, as predicted by Kawashima et al. (personal communication) on the basis of sequence alignment.

The presence of a disulfide bond at the *T. thermophilus* EF-Ts dimer interface raises a possibility for additional stabilization of the functional dimer at higher temperatures. However, experimental evidence for temperature-dependent changes of the redox potential or of enzyme-catalyzed disulfide formation is not available.

ACKNOWLEDGMENT

We thank S. Ealick of CHESS and L. Berman of NSLS for providing access to and help with the A1 and X25 beamline facilities, respectively. We also thank G. Van Duyne and other members of the Sigler laboratory for their general advice and assistance during data collection. We are also grateful to J. Blank for help with protein purification, to M. Meyering-Voss for early crystallization experiments, and to T. Kamashima of the EMBL-Grenoble for helpful discussion. We thank the Alexander Humboldt Foundation for supporting this collaboration through a Visiting Scientist Award to P.B.S.

REFERENCES

An, G., Bendiak, D. S., Mamelak, L. A., & Friesen, J. D. (1981) *Nucleic Acids Res. 9*, 4163−4172.
Arai, K. I., Kawakita, M., & Kaziro, Y. (1972) *J. Biol. Chem. 247*, 7029−7037.
Arai, K. I., Kawakita, M., & Kaziro, Y. (1974a) *J. Biochem. 76*, 293−306.
Arai, K. I., Kawakita, M., Nakamura, S., Ishikawa, I., & Kaziro,Y. (1974b) *J. Biochem. 76*, 523−534.
Arai, K. I., Ota, Y., Arai, N., Nakamura, S., Henneke, C., Oshima, T., & Kaziro, Y. (1978) *Eur. J. Biochem. 92*, 509−543.
Berchtold, H., Reshetnikova, L., Reiser, C. O. A., Schirmer, N. K., Sprinzl, M., & Hilgenfeld, R. (1993) *Nature 365*, 126−132.
Blank, J., Grillenbeck, N. W., Kreutzer, R., & Sprinzl, M. (1995) *Protein Expression Purif. 6*, 637−645.
Blank, J., Nock, S., Kreutzer, R., & Sprinzl, M. (1996) *Eur. J. Biochem. 236*, 222−227.
Bøgestrand, S., Wiborg, O., Thirup, S., & Nyborg, J. (1995) *FEBS Lett. 368*, 49−54.
Bourne, H. R., Sanders, D. A., & McCormick, F. (1990) *Nature 348*, 125−132.
Bourne, H. R., Sanders, D. A., & McCormick, F. (1991) *Nature 349*, 117−127.
Brunger, A. T. (1992) *X-PLOR Version 3.1. A System for X-ray Crystallography and NMR*, Yale University Press, New Haven, CT.
Chevalier, C., Saillard, C., & Bove, J. M. (1990) *J. Bacteriol. 172*, 2693−2703.
Eccleston, J. F., Kanagasabai, T. F., & Geeves, M. A. (1988) *J. Biol. Chem. 263*, 4668−4672.
Jones, T. A., Cowan, S., Zou, J. Y., & Kjeldgaard, M. (1991) *Acta Crystallogr. A46*, 110−119.
Jurnak, F. (1985) *Science 230*, 32−36.
Kawashima, T., Berthet-Colominas, C., Wulff, M., Cusack, S., & Leberman, R. (1996) *Nature 379*, 511−518.
Kjeldgaard, M., & Nyborg, J. (1992) *J. Mol. Biol. 223*, 721−742.
Kjeldgaard, M., Nissen, P., Thirup, S., & Nyborg, J. (1993) *Structure 1*, 35−50.
Kostrzewa, M., & Zetsche, K. (1993) *Plant Mol. Biol. 23*, 67−76.
Kunkel, T. A., Roberts, J. D., & Zakour, R. A. (1987) *Methods Enzymol. 154*, 367−382.
Miller, D. L., & Weissbach, H. (1977) in *Molecular Mechanisms of Protein Biosynthesis* (Weissbach, H., & Pestka, S., Eds.) pp 323−373, Academic Press, New York.
Nissen, P., Kjeldgaard, M., Thirup, S., Polekhina, G., Reshetnikova, L., Clark, B. F. C., & Nyborg, J. (1995) *Science 270*, 1464−1472.
Otwinowski, Z. (1991) *ML-PHARE CCP4 Proc.* 80−88, Daresbury Laboratory, Warrington, U.K.

Otwinowski, Z. (1993) Oscillation Data Reduction Program, in *Proceedings of the CCP4 Study Weekend: Data Collection and Processing* (Sawyer, L., Isaacs, N., & Bailey, S., Eds.) pp 56−62, SERC Daresbury Laboratory, England.

Read, R. J. (1986) *Acta Crystallogr. A42*, 140−149.

Romero, G., Chau, V., & Biltonen, R. L. (1985) *J. Biol. Chem. 260*, 6167−6174.

Ruusala, T., Ehrenberg, M., & Kurland, C. G. (1982) *EMBO J. 1*, 75−78.

Sambrook, J., Fritsch, E. F., & Maniatis, T. (1989) *Molecular Cloning: A Laboratory Manual*, Cold Spring Harbor Laboratory Press, New York.

Sarkar, G., & Sommer, S. S. (1990) *Biotechniques 8*, 404−407.

Sheldrick, G. M. (1990) *Acta Crystallogr. A46*, 467−473.

Sprinzl, M., & Hilgenfeld, R. (1993) in *The Translational Apparatus* (Nierhaus, K. H., et al., Eds.) Plenum Press, New York.

Studier, F. W., Rosenberg, A. H., Dunn, J. J., & Dubendorff, J. W. (1990) *Methods Enzymol. 185*, 60−89.

Wittinghofer, A., Guariguata, R., & Leberman, R. (1983) *J. Bacteriol. 153*, 1266−1271.

Xin, H., Woriax, V., Burkhart, W., & Spremulli, L. L. (1995) *J. Biol. Chem. 270*, 17243−17249.

BI960918W